



This is a repository copy of *Oxygen non-stoichiometry, conductivity and gas sensor response of SnO<sub>2</sub> pellets*.

White Rose Research Online URL for this paper:  
<http://eprints.whiterose.ac.uk/92550/>

Version: Accepted Version

---

**Article:**

Alagdal, I.A. and West, A.R. (2015) Oxygen non-stoichiometry, conductivity and gas sensor response of SnO<sub>2</sub> pellets. *Journal of Materials Chemistry A*, 3 (46). 23213 -23219. ISSN 2050-7488

<https://doi.org/10.1039/c5ta05818j>

---

**Reuse**

Unless indicated otherwise, fulltext items are protected by copyright with all rights reserved. The copyright exception in section 29 of the Copyright, Designs and Patents Act 1988 allows the making of a single copy solely for the purpose of non-commercial research or private study within the limits of fair dealing. The publisher or other rights-holder may allow further reproduction and re-use of this version - refer to the White Rose Research Online record for this item. Where records identify the publisher as the copyright holder, users can verify any specific terms of use on the publisher's website.

**Takedown**

If you consider content in White Rose Research Online to be in breach of UK law, please notify us by emailing [eprints@whiterose.ac.uk](mailto:eprints@whiterose.ac.uk) including the URL of the record and the reason for the withdrawal request.



[eprints@whiterose.ac.uk](mailto:eprints@whiterose.ac.uk)  
<https://eprints.whiterose.ac.uk/>

# Oxygen Non-stoichiometry, Conductivity and Gas Sensor Response of SnO<sub>2</sub> Pellets

Ibtessam A Alagdal and Anthony R West

University of Sheffield  
Dept of Material Science and Engineering  
Mappin Street  
Sheffield S1 3JD  
United Kingdom

## ABSTRACT

*SnO<sub>2</sub> pellets lose a very small amount of oxygen at high temperatures to give, for instance, the stoichiometry SnO<sub>1.9989(1)</sub> at 1200 °C in air. The oxygen deficiency,  $\delta$  can be preserved at ambient temperature in quenched samples. The level of conductivity, which is n-type, depends on oxygen content,  $2-\delta$  and varies by several orders of magnitude; activation energies cover the range 1.1 eV for slow-cooled, fully oxidised samples to 0.52 eV for samples quenched from 1200 °C. Quenched samples can be readily and reversibly reoxidised and reduced at temperatures as low as 700 °C; at lower temperatures, down to ~ 350 °C, oxidation and reduction is mainly confined to sample surfaces on short timescales but, nevertheless, is sufficient for the conductivity to change by 1 to 2 orders of magnitude. Quenched, oxygen-deficient samples are also moisture-sensitive whereas fully oxidised samples are not. SnO<sub>2</sub> shows similar sensitivity to both CO<sub>2</sub> and N<sub>2</sub>, which is attributed to loss of O<sub>2</sub> from the sample surface.*

## INTRODUCTION

Tin oxide, SnO<sub>2</sub>, both pure and doped, has many applications as a functional material which can be grouped into three main areas, as a (i) a solid state gas sensor, (ii) an oxidation catalyst and (iii) a transparent conducting oxide, TCO<sup>1-3</sup>. The first two applications are surface-driven whereas TCO's are used for their bulk properties.

For surface-driven applications, sample fabrication is important and SnO<sub>2</sub> has been prepared in many forms and by various methods including, as examples, porous materials,<sup>4</sup> sol-gel derived nano particles<sup>5</sup>, inductively-coupled plasma nanorods<sup>6</sup>, dc magnetron-deposited thin films together with Pt, Pd catalyst particles on the surface<sup>7</sup>, hydrothermally-prepared nanoplatelets<sup>8</sup> and electrochemically-anodised films<sup>9</sup>. The nature and mechanism of gas-surface interactions are key to the use of

SnO<sub>2</sub> as both a catalyst in industrial oxidative dehydrogenation and as a sensor of reducing gases. Nevertheless, the mechanistic details are still a matter of debate, especially the effects of O<sub>2</sub> and H<sub>2</sub>O on the sensor conductivity.

There are numerous comments in the literature<sup>10-12</sup> about the possibility of oxygen non-stoichiometry, with the formula SnO<sub>2-δ</sub>, but the value(s) of δ and its possible dependence on sample processing conditions has not been quantified. It is stated that a key method to introduce oxygen vacancies into SnO<sub>2</sub> is to use a divalent tin compound, SnCl<sub>2</sub>·2H<sub>2</sub>O, as the precursor in hydrothermal synthesis<sup>10</sup>, with evidence for oxygen vacancies obtained by both X-ray photoelectron spectroscopy, XPS and electron spin resonance, ESR, spectroscopy. The electrical conductivity of SnO<sub>2-δ</sub> is n-type whereas that of the oxygen-rich divalent oxide, SnO<sub>1+δ</sub> is p-type<sup>11</sup>. Instances of p-type conductivity in SnO<sub>2</sub> films have been attributed to the presence of SnO-like regions within films that were shown to be inhomogeneous<sup>11</sup> and contained both SnO<sub>2</sub>- and SnO-like regions.

Impedance spectroscopy, IS, has been used to characterise SnO<sub>2</sub> films prepared by two methods, rf magnetron sputtering of thin films and doctor blade deposition of thick films followed by heating in air at 500 °C for 2 hrs<sup>12</sup>. Using IS, the sensitivity of the films to N<sub>2</sub>/O<sub>2</sub> at 150 and 200 °C was studied; film resistance increased in O<sub>2</sub> and decreased in N<sub>2</sub>, consistent with n-type behaviour.

Several studies of the effect of H<sub>2</sub>O adsorption on SnO<sub>2</sub> have been reported<sup>13-20</sup>. Different mechanisms of SnO<sub>2</sub> - H<sub>2</sub>O interaction have been proposed, depending on the structure of the SnO<sub>2</sub> surface and explanations given for the observed changes in conductivity. For instance, it was suggested that absorption of H<sub>2</sub>O leads to band-bending within the SnO<sub>2</sub> electronic structure and an associated increase in conductivity<sup>13</sup>.

The interaction of SnO<sub>2</sub> surfaces with O<sub>2</sub>, H<sub>2</sub>O and H<sub>2</sub> was investigated by temperature programmed desorption, TPD, chromatography<sup>14</sup>. Evidence was found for four kinds of oxygen species which desorbed at 80 °C (O<sub>2</sub>), 150 °C (O<sub>2</sub><sup>-</sup>), 560 °C (O<sup>-</sup> or O<sup>2-</sup>) and > 600 °C (lattice O<sup>2-</sup>). O<sub>2</sub><sup>-</sup>, O<sup>-</sup> and O<sup>2-</sup> were described as *depletive adsorbates* since on desorption, electrons were released (together with gaseous O<sub>2</sub>) leading to an increase in conductivity. Two kinds of adsorbed H<sub>2</sub>O species were identified similarly by TPD, at 100 °C (molecular H<sub>2</sub>O) and 400 °C (OH groups). Release of OH groups, but not H<sub>2</sub>O molecules, was accompanied by a decrease in conductivity although the mechanism responsible for the change in conductivity was not clear<sup>14</sup>.

The main purposes of the present work were: first, to establish whether SnO<sub>2</sub> showed a temperature-dependent variation in oxygen content of the kind shown by rutile, TiO<sub>2</sub> which has the same crystal structure as SnO<sub>2</sub><sup>21</sup>; second, to determine the conductivity of SnO<sub>2</sub> pellets as a function of any oxygen non-stoichiometry and sample processing conditions; third, to establish the effect of possible oxygen non-stoichiometry on sensitivity to O<sub>2</sub>, N<sub>2</sub>, CO<sub>2</sub> and H<sub>2</sub>O.

## EXPERIMENTAL

High purity SnO<sub>2</sub> (99.9 % Sigma Aldrich) was ground to a fine powder with an agate mortar and pestle, pressed into pellets of 20 mm diameter at 0.6 tonnes, placed on sacrificial SnO<sub>2</sub> powder in a Pt crucible and fired at 1300 °C for 8 hrs in air. The sintered pellets were then given subsequent heat treatments, either at temperatures in the range 800 to 1200 °C in air for 2 hours followed by quenching to room temperature (by removing from the furnace and allowing to cool in air, typically over a period of 1-2 mins), or at 900 °C in O<sub>2</sub> for 2 hrs followed by slow cool in O<sub>2</sub> to room temperature (by switching off the furnace). Typical pellet densities were 50-62 % with a porous microstructure consisting of interconnected grains of size ~ 0.5 – 2.5 μm, Fig 1.

Pellets for IS measurements were coated with Pt paste on opposite faces which was dried and hardened at 900 °C for 1 hr to form electrodes. These were attached to Pt leads in a conductivity jig, which was placed inside a horizontal tube furnace through which different gases could be passed, allowed to equilibrate, typically for 10 – 30 mins and then IS data recorded. In general, Pt electrodes were fabricated before the final heat treatments to avoid possible unwanted oxidation/reduction prior to the IS measurements. Measurements were made isothermally in the temperature range 200 to 700 °C and over the frequency range 10 Hz to 1 MHz using Hewlett Packard 4192A instrumentation. Impedance data were corrected for overall pellet geometry and are reported in units of resistance: ohm cm and capacitance : F cm<sup>-1</sup>; data were not corrected for the geometry of regions such as grain boundaries since this was not known accurately.

In order to measure changes in sample mass as a function of temperature, thermogravimetry, TG, could not be used as the mass changes (a few micrograms) were too small to be detected reliably with available TG instrumentation. Instead, the mass of a pellet of approximately 2 g was measured on a microbalance after a range of heat treatments. The same pellet was placed in a Pt boat, heated isothermally for 1 hr over the range 25 – 1200 °C, cooled rapidly to room temperature and its mass recorded before returning to the furnace. Data were obtained stepwise on both heating and cooling.

## RESULTS and DISCUSSION

All pellets used for the results reported here were sintered initially at 1300°C for 8 hrs in air and then given a range of follow-on heat treatments. X-ray powder diffraction, XRD, on crushed pellet fragments confirmed that the samples were phase-pure SnO<sub>2</sub> with the rutile structure after various heat treatments. Detection of secondary phases by XRD is typically at the 1-2% level and the technique is therefore insensitive to, for instance, any small changes in surface structure or composition.

For weight change studies, a pellet of mass ~ 2 g was given a second heating at 900 °C in O<sub>2</sub> for 2 h, slow-cooled to room temperature and then reheated in air isothermally at different temperatures, quenched to room temperature and its mass recorded. Data are summarised in Fig 2 for stepwise heating and cooling of the same sample. In order to assign values of  $\delta$  to the oxygen contents, it was assumed that the sample cooled stepwise to room temperature was oxygen-stoichiometric SnO<sub>2</sub>. The right hand ordinate of Fig. 2 is therefore an oxygen content scale.

Fully reversible data were obtained over the range 700 – 1200 °C and are attributed to variation in oxygen content as a function of temperature in air. At lower temperatures, data were not reversible on the heat/cool cycle. An initial decrease in weight occurred at 200 °C which was attributable to loss of H<sub>2</sub>O absorbed during the slow cool from 900 °C. The weight then increased again at 600 and 700 °C; this was attributed to uptake of O<sub>2</sub> by the sample that was still slightly oxygen-deficient, in spite of its slow cool in O<sub>2</sub> from 900 °C. Above 700 °C, the sample started to lose weight again and this continued to the highest temperature studied, 1200 °C.

From these experiments, it is concluded that :

(i) SnO<sub>2</sub> loses oxygen spontaneously and reversibly in air over the temperature range 700 to 1200 °C. At 1200 °C, for instance, its oxygen content is given by the formula SnO<sub>1.9989(1)</sub>. Oxygen-deficient SnO<sub>2</sub> is expected to be an n-type semiconductor whose conductivity is sensitive to pO<sub>2</sub> and is given by the mechanism:



(ii) The rate of uptake of O<sub>2</sub> by oxygen-deficient SnO<sub>2- $\delta$</sub>  during cooling is very temperature-dependent. Equilibrium is readily obtained down to 700 °C, but prolonged isothermal heating is required to achieve full, internal equilibrium at lower temperatures, although the gas-solid surface reactions proceed much more rapidly than those requiring diffusion into sample interiors. Several stages in the uptake and desorption of O<sub>2</sub> may be envisaged.

(iii) Oxygen-deficient  $\text{SnO}_{2-\delta}$  is moisture-sensitive and, at lower temperatures, uptake of  $\text{H}_2\text{O}$  may take place more easily than uptake of  $\text{O}_2$ . It is presumed that  $\text{H}_2\text{O}$  uptake occurs by the reaction:



(iv) The stoichiometry of both the surface and interior of  $\text{SnO}_2$  pellets depends critically on the final cooling step, especially cooling rate and atmosphere. Thus, the overall level of oxygen deficiency,  $\delta$ , may vary but in addition, concentration gradients in  $\delta$  may exist, in which surfaces have smaller  $\delta$  than grain interiors, especially if oxidation and equilibration are incomplete at a particular temperature. Similarly, gradients in concentration of adsorbed  $\text{H}_2\text{O}$  may be present on short exposure timescales. In order to assess the possible significance of these stoichiometry variations on electrical properties, IS measurements were made on pellets given a range of heat treatments.

Impedance data for a typical sample, with measurements at several temperatures, are shown in Fig 3. Data are presented in various ways to highlight different impedance characteristics of the sample and to allow a more comprehensive understanding of its electrical make-up and properties<sup>22</sup>. There are four widely-used impedance formalisms, the impedance,  $Z^*$ , the admittance,  $Y^*$  (or  $A^*$ ), the modulus,  $M^*$  and the permittivity,  $(\epsilon^*)$ . These are inter-related by:

$$Z^* = (Y^*)^{-1} = (j\omega C_0)^{-1} M^* = (j\omega C_0 \epsilon^*)^{-1} \quad (3)$$

where  $\omega$  is the angular frequency,  $2\pi f$  and  $C_0$  is the vacuum capacitance of the sample. Data can be presented in any of the four formalisms, either as complex plane plots or as spectroscopic plots of one parameter against frequency. It is certainly not necessary to present data in all possible ways, but we find that the combination of plots used in Fig 3 usually permits a comprehensive overview of the electrical microstructure of a sample to be obtained.

Thus, for the data shown in Fig 3, complex plane plots,  $Z''$  vs  $Z'$ , (a), show a single, broad arc whose low frequency intercept on the  $Z'$  axis gives the total resistance of the sample,  $R_T$ . On replotting the same data as  $\log Y'$  vs  $\log f$ , (b), a low frequency plateau is seen with a conductivity value  $R_T^{-1}$  and a dispersion at high frequencies which moves off-scale with increasing temperature. These high frequency data show a power law dependence of  $\log Y'$  on  $\log f$  and are an example of Jonscher's law of universal dielectric response<sup>23</sup> that is observed in many ionic and electronic conductors.

The same data replotted as  $\log C'$  vs  $\log f$ , (c), show two plateaux with approximate values 3 and 20 pF whose interpretation is that the sample response contains both bulk (grain) and grain boundary impedances. Thus, a value of  $\sim 3$  pF for the high frequency plateau corresponds to a permittivity of  $\sim 34$  and is attributed to the sample bulk. The magnitude of the low frequency plateau is rather small for a conventional grain boundary of a well-sintered ceramic which suggests that it occupies a significant volume fraction of the sample. SEM data, Fig 1, show a porous microstructure of interconnected grains and the low frequency capacitance plateau is therefore attributed to a constriction resistance associated with the necks between adjacent grains together with the air gaps between grains<sup>24</sup>. Since the same material is usually present in the necks and grains, a characteristic feature of constriction resistances is that the activation energies of the grain and grain boundary resistances are similar.

A useful, pictorial overview of the electrical microstructure of the sample is obtained by replotting the same data as  $M''/Z''$  vs  $\log f$  (d); this type of presentation is also known as impedance and modulus spectroscopy<sup>25</sup>. A single peak is seen in the  $M''$  spectrum which represents the smallest capacitance in the sample; this therefore, corresponds to the bulk impedance. The  $Z''$  peak, scaled to be of similar height to the  $M''$  peak for an easy visual assessment, occurs at similar, but slightly lower, frequency and additionally, contains a low frequency, poorly-resolved shoulder peak. The main  $Z''$  peak therefore represents the bulk resistance as it overlaps with the  $M''$  peak. The low frequency shoulder peak is the grain boundary resistance associated with the low frequency plateau seen more clearly in (c).

The small difference in peak maximum frequencies between the  $Z''$  and  $M''$  peaks is associated mainly with the constant phase element, CPE, in the equivalent circuit, Fig 4, that is used to model the impedance data. The admittance of the bulk element,  $R_1$ - $C_1$ -CPE<sub>1</sub> in the circuit shown in Fig 4 is given by <sup>26</sup>:

$$Y^* = (R_1)^{-1} + j\omega C_1 + A_1\omega^n + jB_1\omega^n \quad (4)$$

$$\text{where } (A_1/B_1) = \tan(n\pi/2) \quad (5)$$

The CPE is, effectively, a parallel combination of a frequency-dependent resistor and capacitor; the relative contribution of each to the overall, frequency-dependent admittance is governed by the power law exponent,  $n$ <sup>27</sup>.

The effect of including a CPE in the equivalent circuit may be seen by comparing the resulting impedance with that of an ideal parallel RC element, without a CPE, whose admittance is given by:

$$Y^* = (R)^{-1} + j\omega C \quad (6)$$

The resulting  $M''$  and  $Z''$  spectra of an ideal RC element consist of symmetric 'Debye peaks' with the functional form:

$$\text{Peak profile} = \frac{\omega RC}{1+(\omega RC)^2} \quad (7)$$

and for which the peak maxima are given by:

$$\omega RC = 1 \quad (8)$$

The peaks are scaled according to  $(C_o/C)$  for  $M''$  and  $R$  for  $Z''$ <sup>22</sup>. On introduction of a CPE in the equivalent circuit, characteristic changes are that (i) the  $M''$  peak occurs at slightly higher frequency than the  $Z''$  peak, (ii) the  $M''$  peak is Debye-like on the low frequency side but broadened asymmetrically on the high frequency side and conversely, (iii) the  $Z''$  peak is broadened at low frequencies but Debye-like at high frequencies<sup>26</sup>.

From the impedance data shown in Fig 3 and their interpretation in terms of the equivalent circuit shown in Fig 4, the electrical microstructure of the SnO<sub>2</sub> pellets **appears to have** the following characteristics:

- (i) the total sample resistance is a combination of grain and grain boundary resistances connected in series.
- (ii) the grain boundary impedance is the neck region connecting grains in the poorly-sintered, porous sample and is a constriction impedance.

The implication from this analysis is that the measured impedance represents that of the sample volume, not its surface. **There was no evidence for the possible existence of a core-shell structure with conducting grains surrounded by resistive grain boundaries or surfaces. Thus, the high frequency capacitance data, Fig 3(c), show no evidence of a downturn to an additional plateau at still higher frequencies; similarly, the  $Y'$  data show no evidence of an additional plateau of much higher conductivity at the highest frequencies. Both of these should have been apparent in the  $C'$ ,  $Y'$  data if the materials had conductive grain cores. In addition, the magnitude of the high frequency  $C'$  plateau is consistent with that expected for the bulk response of SnO<sub>2</sub>.** This interpretation is therefore used in the following analyses.



Total conductivity data were obtained either from the low frequency intercept on the  $Z'$  axis of the impedance complex plane plots, Fig 3(a) or from the low frequency  $Y'$  plateaux (b). Approximate values for the bulk conductivity were obtained from the  $M''$  spectra using equation 8 for the peak maximum frequency and equation 9 for the peak height:

$$M''_{\max} = C_o/2C \quad (9)$$

Bulk,  $\sigma_b$  and total,  $\sigma_T$  conductivity data for a range of samples are shown in Fig 5. Slow-cooled samples were measured in  $O_2$  to avoid possible  $O_2$  loss during the impedance measurements. By contrast, quenched samples were measured in  $N_2$  to avoid possible oxidation during IS measurement. Conductivities were highest for samples quenched from the highest temperature, 1200 °C and lowest for samples slow-cooled in  $O_2$ ; activation energies ranged from 0.52 to 1.10 eV. These data are fully consistent with n-type conduction that is controlled by the degree of oxygen nonstoichiometry,  $\delta$ , Fig 2. Large changes in conductivity occur for very small changes in  $\delta$ . Although the changes in  $\delta$  are initiated by gas-solid reactions at sample surfaces, equation 1, the conductivities appear to be controlled by sample interiors rather than surfaces since both bulk and grain boundary components are detected in the impedance response, Fig 3. The bulk conductivities in Fig 5(a) are higher than the total conductivities, (b), and have slightly smaller activation energies. The **higher activation energy of the total conductivity** reflects the contribution of the grain boundaries to the total impedance, especially at lower temperatures: **since the grain boundaries are generally more oxidised than the grains, they have smaller  $\delta$  values and higher activation energies, as shown by the decrease in activation energy with increased reduction at higher quench temperature in Fig 5(a).**

Changes in sample mass due to oxygen loss/gain were detected at temperatures as low as 600 °C, Fig 2; however, conductivity measurements in different atmospheres showed evidence of oxygen loss/gain at much lower temperatures, Fig 6. At eg 350 °C, the total conductivity of a sample slow-cooled in  $O_2$  increased gradually by > 1 order of magnitude on changing the atmosphere to  $N_2$ . The initial conductivity was subsequently recovered by switching back to  $O_2$ ; similar conductivity changes occurred more rapidly with increasing temperature. These conductivity changes, by 1-2 orders of magnitude, are less than the total range of conductivities, covering 4-5 orders of magnitude, that are obtainable at a particular temperature from variation in  $\delta$ , Fig 5. The initial conductivity changes are clearly surface-controlled, therefore, **whereas those that include** exchange of species, such as oxygen vacancies, between sample interior and surface are important on longer time scales.

Conductivity data were also sensitive to moisture in the atmosphere, as shown in Fig 7 on changing the atmosphere between wet and dry N<sub>2</sub> at 300 °C for an oxygen-deficient sample prepared by quenching from 1000 °C. Conductivity increased by > 1 order of magnitude in wet N<sub>2</sub> with an associated reduction in activation energy. Sensitivity to moisture was, however, greatly dependent on sample history, as summarised in Fig 8 for quenched and slow-cooled samples measured in wet/dry N<sub>2</sub>: the quenched sample was sensitive to moisture whereas the slow-cooled sample was not.

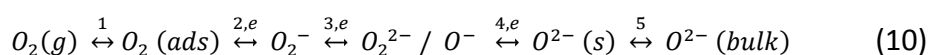
At present, we cannot comment on whether increased conductivity in a wet atmosphere is electronic or protonic. Proton conductivity certainly seems to be a possibility since proton conductivity at high temperature in doped cerate perovskite structures is well-established<sup>28</sup> and is attributed to proton transfer associated with OH groups that form on adsorption of H<sub>2</sub>O by oxygen-deficient samples. However, there are comments in the literature concerning possible modification in the level of electronic conductivity and the band structure at the SnO<sub>2</sub> surface associated with water adsorption / desorption; further work is therefore required to determine the nature of the conducting species associated with H<sub>2</sub>O adsorption.

It is important to understand the electronic and (possible) protonic contributions to the overall conductivity of a particular SnO<sub>2</sub> sample and how they vary depending on sample processing conditions and the atmosphere prior to and during, IS measurements. This is illustrated further by the changes seen on varying the atmosphere between dry and wet O<sub>2</sub>, N<sub>2</sub> and CO<sub>2</sub> in Fig 9 at 400 °C. In O<sub>2</sub>, the conductivity increased only slightly between dry and wet atmosphere. In dry N<sub>2</sub> or CO<sub>2</sub>, the conductivity increased reversibly by 1-2 orders of magnitude and by an additional 1-2 orders of magnitude on switching to wet atmospheres. The first increase, in dry atmospheres, can be attributed to increased electronic conduction associated with loss of O<sub>2</sub> on reducing pO<sub>2</sub> in the surrounding atmosphere. The second increase, on changing to a wet atmosphere, may be due to proton conduction or alternatively, to electronic conduction if the SnO<sub>2</sub> band structure changes on H<sub>2</sub>O uptake.

These results obtained in dry atmospheres show that conductivity changes seen in CO<sub>2</sub> are attributable directly to changes in  $\delta$  since similar results are seen in both N<sub>2</sub> and CO<sub>2</sub>. SnO<sub>2</sub> is therefore only an indirect sensor of CO<sub>2</sub>, as the sensing mechanism involves exchange of O<sub>2</sub> between the sample and the surrounding atmosphere and not direct interaction between CO<sub>2</sub> and SnO<sub>2</sub>. Furthermore, these results show the importance of oxygen vacancies in order for H<sub>2</sub>O adsorption to occur, but also, that oxygen vacancies can be created during the conductivity measurements. Thus, in a

moist N<sub>2</sub> atmosphere, desorption of O<sub>2</sub> may occur, allowing subsequent absorption of H<sub>2</sub>O by the mechanism shown in equation (2).

The changes in electronic conductivity associated with adsorption/desorption of O<sub>2</sub> are represented simplistically by equation (1) but in reality, a much more complex sequence of processes is likely to occur, involving a series of equilibria that can be displaced in either direction, depending on pO<sub>2</sub>, as follows:



where *g*, *ads* and *s* refer to gas phase, adsorbed species and surface. Equilibria 1 and 5 do not involve electron transfer, but any of equilibria 2, 3 and 4 should be detected by IS since, although the equilibria involve reactions at the gas-solid interface, electrons are likely to be withdrawn from/added to the sample interior as part of the redox reactions. Evidence for the different oxygen species at sample surfaces, which are involved in the equilibria shown in (10), was obtained from TPD studies<sup>14</sup> which showed that **increasingly higher** temperatures were required to release species adsorbed as O<sub>2</sub> (g), O<sub>2</sub><sup>-</sup>, O<sup>-</sup>/O<sup>2-</sup> and O<sup>2-</sup> (bulk). **This is entirely consistent with our conclusion that step 5, leading to full equilibration of oxygen stoichiometry and distribution throughout the sample bulk, requires temperatures above 600-700 °C for it to be achieved on reasonable timescales.**

Although changes to the equilibria 2, 3 and 4 would be detected by IS, an additional possibility that would probably not be detected by IS involves electron transfer between underbonded lattice O<sup>2-</sup> ions and adsorbed oxygen molecules, as in:



**The resulting O<sup>-</sup> ions may then act as sources of hole conduction.** Hole conductivity associated with **the location of holes on oxygen as O<sup>-</sup> ions** in acceptor-doped titanate perovskites<sup>29</sup>, Ca-doped BiFeO<sub>3</sub><sup>30</sup> and yttria-stabilised zirconia<sup>31</sup> has been attributed to electron transfer processes involving underbonded oxide ions. Hence, the equilibria shown in (11) provide a **modification** to step 2 in (10), **by assigning the source of** electrons involved in the redox process to underbonded O<sup>2-</sup> ions rather than to those associated with the n-type conduction mechanism. **Reactions such as (11) could occur at SnO<sub>2</sub> surfaces and involve underbonded oxide ions that are not surrounded by a full complement of positive (cation) charge and indeed, evidence for species such as O<sup>-</sup> and O<sub>2</sub><sup>-</sup> is widely cited in surface science studies<sup>32</sup>.**

**The literature contains very many reports on SnO<sub>2</sub> gas sensors, the variety of atomic and molecular steps that occur at sensor surfaces, the effect of sensor**

microstructure and the nature of sample – electrode contacts, all of which have been reviewed<sup>3,32</sup>. *ac* impedance measurements have also been used on numerous occasions<sup>33-35</sup> and resistivity changes associated with change in oxygen pressure have been reported<sup>36,37</sup>. The novelty of the present work concerns impedance measurements as a function of temperature and atmosphere on carefully-prepared samples with different oxygen contents. From our results, it appears that the conductivity that is measured is a combination of grain and grain boundary conductivities associated with the sample bulk, even though sensing action involves gas-solid interactions at sample surfaces.

Models for sensing action that are discussed in the literature frequently are based on the creation of Schottky barriers and depletion layers. We find no evidence for Schottky barriers since our impedance data can be satisfactorily interpreted in terms of low-capacitance bulk and grain boundary impedances: Schottky barriers at sample-electrode interfaces would lead to additional thin layer impedances with associated capacitances typically in the nanoFarad range, in contrast to the picoFarad range of capacitances observed here. It would, however, be useful to confirm this conclusion by I-V measurements.

The concept of depletion layers may usefully be applied in our case since O<sub>2</sub> absorption at sample surfaces is associated with electron withdrawal from sample interiors, leading to positively-charged depletion layers. However, we see no evidence in the impedance data for conducting grain cores surrounded by more resistive depletion layers; the implication of this is that the depletion layer thickness is greater than the sizes of the grains.

## CONCLUSIONS

SnO<sub>2</sub> pellets show a small, reversible loss of oxygen, in air, at temperatures above about 600 °C. Samples also lose oxygen reversibly at lower temperatures, eg 350 °C, simply by switching the atmosphere between O<sub>2</sub> and N<sub>2</sub>, but the changes are confined to sample surfaces, at least on short timescales. The weight changes, which are detectable using a microbalance and a 2 g pellet, cause a change in *n*-type conductivity by several orders of magnitude, depending on the level of oxygen nonstoichiometry,  $\delta$ .

Sample conductivity, and its sensitivity to gases, **depends critically on** the sample history. Thus, quenched, oxygen-deficient samples are sensitive to moisture uptake whereas slow-cooled, oxygen-stoichiometric samples are not. CO<sub>2</sub> and N<sub>2</sub> show a similar sensor response, attributable to desorption of O<sub>2</sub> in both cases.

Impedance spectroscopy provides evidence for grain and grain boundary contributions to the overall sample impedance, both of which show a similar sensor response. Although the sensor response involves gas – solid surface reactions, it appears that the measured conductivity changes are bulk conductivities and not surface conductivities.

#### ACKNOWLEDGEMENTS

IAA thanks the Libyan Embassy for financial support

#### REFERENCES

1. D.E. Williams in 'Solid State Gas Sensing' ed. P.T. Moseley and B.C. Tofield, Adam Hilger, Bristol (1987)
2. V.E. Henrich and P.A. Cox, 'The surface science of metal oxides', Cambridge University, Press (1994)
3. M. Batzill and U. Diebold, *Progr. Surf. Sci.*, **79** (2005) 47
4. H-C. Shin, J. Dong and M. Liu, *Adv. Mater.*, **16** (2004) 237
5. F. Morazzoni *et al*, *Mater. Sci. Eng.*, **C15** (2001) 167
6. A. Forleo *et al*, *Procedia Chemistry*, **1** (2009) 196
7. E.Y. Sevastyanov *et al*, *Semiconductors*, **46** (2012) 801
8. Y.Z. Zhang *et al*, *Int. J. Electrochem. Sci.*, **8** (2013) 3371
9. A. Yamaguchi *et al*, *Thin Solid Films*, **519** (2011) 2415
10. J. Pan *et al*, *Chem. Commun.*, **50** (2014) 7020
11. S. Hwang *et al*, *J. Amer. Ceram. Soc.*, **95** (2012) 324
12. R. Savu *et al*, *Mater. Res.*, **12** (2009) 83
13. M. Batzill, W. Bergermayer, I. Tanaka and U. Diebold, *Surf. Sci.*, **600** (2006) L29
14. N. Yamazoe, J. Fuchigami, M. Kishikawa and T. Seiyama, *Surf. Sci.*, **86** (1979) 335
15. N. Barsan and R. Ionescu, *Sensors and Actuators* **B12** (1993) 71
16. V.A. Gercher and D.F. Cox, *Surf. Sci.*, **322** (1995) 177
17. G. Korotchenkov, V. Brynzari and S. Dmitriev, *Sensors and Actuators*, **B54** (1999) 197.
18. T.F. McAleer, P.T. Moseley, J.O.W. Norris and D. E. Williams, *Faraday Trans.*, **83** (1987) 1323.
19. J. Tamaki *et al*, *Surf. Sci.*, **221** (1989) 183.
20. K. Watanabe *et al*, IMCS 2012 – The 14<sup>th</sup> Int. meeting on chemical sensors, DOI 10.5162/IMCS 2012/P.2.0.9, 1285.
21. Y. Liu and A. R. West, *J Amer. Ceram. Soc.*, **96** (2013) 218.
22. J.T.S. Irvine, D.C. Sinclair and A.R. West, *Adv. Mater.*, **2** (1990) 132
23. A.K. Jonscher, *Dielectric relaxation in solids*, Chelsea Dielectrics Press, London, (1983)

24. P.G. Bruce and A.R. West, *J. Electrochem. Soc.*, **130** (1983) 662
25. I.M. Hodge, M.D. Ingram and A.R. West, *J. Electroanal. Chem.*, **74** (1976) 125
26. D.P. Almond and A.R. West, *J. Electroanal. Chem.*, **186** (1985) 17
27. D.P. Almond, C.R. Bowen and D.A.S. Rees, *J. Phys. D, Appl. Phys.*, **39** (2006) 1295
28. H. Uchida *et al*, *Solid State Ionics*, **36** (1989) 89
29. H. Beltran *et al*, *J. Amer. Ceram. Soc.*, **94** (2011) 2951
30. N. Maso *et al*, *Phys. Chem. Chem. Phys.*, **16** (2014) 19408
31. N. Maso and A.R. West, *Chem. Mater.*, **27** (2015) 1552
32. W. Gopel and K.D. Schierbaum, *Sensors and Actuators*, **B26-27** (1995) 12
33. G. Martinelli *et al*, *Sensors and Actuators*, **B26-27** (1995) 53
34. M. Labeau *et al*, *Sensors and Actuators*, **B26-27** (1995) 49
35. U. Weimar and W. Gopel, *Sensors and Actuators* **B26-27** (1995) 13
36. G. Blaustein *et al*, *Sensors and Actuators* **B55** (1999) 33
37. F. Schipani *et al*, *J. Appl. Phys.*, **116** (2014) 194502

#### FIGURE CAPTIONS

1. Microstructure of a typical sintered pellet of SnO<sub>2</sub>
2. Change in mass and oxygen content of SnO<sub>2</sub> as a function of temperature; red crosses: stepwise heating of a sample slow-cooled from 900 °C; yellow squares: stepwise cooling from 1200 °C. **The errors in the mass measurements, +/- 0.00002 g, are within the size of the data points.**
3. A typical impedance data set collected at 5 temperatures
4. Equivalent circuit used to analyse impedance data
5. (a)bulk and (b)total conductivities of SnO<sub>2</sub> pellets given different heat treatments after initial sintering at 1300 °C. All samples were quenched from the temperatures stated apart from 900 SC which was slow-cooled in oxygen from 900 °C
6. Effect of pO<sub>2</sub> in a dry atmosphere on the total conductivity of an SnO<sub>2</sub> pellet prepared by slow cooling from 1000 °C and then held in O<sub>2</sub> for 1 hour before IS measurements
7. Effect of a dry / wet atmosphere on the conductivity, in N<sub>2</sub>, of an SnO<sub>2</sub> pellet quenched from 1000 °C; data recorded at 300 °C
8. Effect of atmosphere, moisture and sample history on conductivity of SnO<sub>2</sub> pellets. SC: slow cool; Q: quenched from 1000 °C
9. Time-dependent response of the **total** conductivity of a **slow-cooled** SnO<sub>2</sub> pellet at 400 °C to a range of dry and wet atmospheres

